Sharif University of Technology

Scientia Iranica

Transactions on Mechanical Engineering

https://scientiairanica.sharif.edu

Vibration analysis of size-dependent higher-order plates based on micropolar theory

Yazdan Alipour [a], Saleh Hamzehei-Javaran [b], Saeed Shojaee [a,*]

a. Department of Civil Engineering, Shahid Bahonar University of Kerman, Kerman, Iran.
b. Faculty of Civil and Environmental Engineering, Tarbiat Modares University, Tehran, Iran.

* Corresponding author: saeed.shojaee@uk.ac.ir (S. Shojaee)

Received 23 December 2022; Received in revised form 19 January 2024; Accepted 22 June 2024

Keywords

Micro-Polar Continuum Theory (MPCT);
Size-dependent plates;
Higher-order elements;
Micro-rotational Degrees of Freedom (DOF);
Mechanical response;
Drilling Degrees of Freedom (DOF);
Finite Element Method (FEM).

Abstract

By considering micro-rotational Degrees of Freedom (DOF), the Micro-Polar Continuum Theory (MPCT) can characterize the effect of micro-structures on the mechanical analysis of material particles, which Classical Theories (CT) of elasticity are unable to describe. The vibration behavior of the higher-order plates with a drilling DOF is discussed in this article to suggest a novel size-dependent rectangular element based on the micropolar elasticity theory. To do this, a new general formulation of the MPCT, which can be employed with ease in the Finite Element Method (FEM), is initially developed. The displacements and micro-rotations are therefore computed using quadratic shape functions on a rectangular plate element. In this element, the proper stiffness and mass matrices for the drilling DOF are derived, and to demonstrate the precision and application of the proposed element, several numerical examples of micropolar plates with various boundary conditions have been carried out. The current finite element formulation shown here is effectively used to take into account the micropolar efficiency for modeling microplates. This research contributes to advancing our understanding of the mechanical response of materials at the microscale.

1. Introduction

The mechanical behavior of small-scale structures is proven to be size-dependent experimentally. As a result, while Classical Theories (CT) is recognized as an effective technique for the study of large-scale structures, it cannot be applied to micro-structure problems. When the micro-structure effect is important during the analysis of materials, higher-order continuum theories are frequently applied. This is due to the fact that they are more accurate and efficient at computing than atomistic methods like Molecular Dynamic (MD) simulations. Several non-classical continuum theories have been established to date in order to capture the small-scale influence on the mechanical behavior of micro- and nano-structures. For instance, several researchers have employed the Strain Gradient Theory (SGT) and Couple Stress Theory (CST) [1,2] as well as the modified versions of these theories (Modified Strain Gradient Theory (MSGT) and Modified Couple Stress Theory (MCST)) to analyze microbeams and microplates behavior [3]. Under classical and elastic boundary conditions, Hou et al. [1] utilized the SGT to examine the vibration characteristics of a thin-walled cylindrical shell, in which natural frequencies measured using strain gradient elasticity theory are shown to be lower than those of the classical shell model. Ahmad et al. [2] presented numerical and analytical solutions to the Stokes theory of couple stress fluid in the inclined channel under the effects of constant, space, and variable viscosity. Based on modified SGT, Gholami and Alizadeh [3] carried out a bending analysis of Functionally Graded (FG) size-dependent beams. Particularly, the literature on the dynamics of micro-structures has a number of publications based on such theories.

To cite this article:
Y. Alipour, S. Hamzehei-Javaran, and S. Shojaee "Vibration analysis of size-dependent higher-order plates based on micropolar theory", *Scientia Iranica* (2025) **32**(11):7388. https://doi.org/10.24200/sci.2024.61589.7388

The Cosserat and Cosserat [4] initiated the higher-order continuum theory known as the micropolar theory in 1909. After almost fifty years, a study rekindled the interest of Eringen and Suhubi [5] in the field of developing MPCT, which is a size-dependent theory that takes into account a rigid micro-structure that may rotate independently from the neighboring medium [6,7] at each material particle in a micropolar continuum. Each material point on the continuum possesses six Degrees of Freedoms (DOFs), including three rotational and three translational ones. Both fluids [8,9] and solids [10-16] may be studied using the Micro-Polar Continuum Theory (MPCT). An MPCT, as proposed by Afsar Khan et al. [8], was employed to analyze the behavior of Magneto-Hydro-Dynamic (MHD) fluid over a curved stretching surface. The study incorporates the Cattaneo-Christov theory of heat diffusion with a novel heat model. A mathematical model was developed by Nadeem et al. [9] using micropolar fluid flows on a Riga plate. Additionally, it has been the focus of several research projects on solid mechanics. In a comprehensive study [11], the micropolar theory and Carrera Unified Formulation (CUF) were employed for finite element analysis, focusing on stationary and axially moving beams. The proposed approach used Taylor-like and Lagrange polynomials, considering material properties graded over the beam's thickness. The formulation of the linearized MPCT was used by Aganovic´ et al. [12] to derive and justify models of microplates mathematically. A Cosserat model that was linear, elastic, static, and isotropic was developed by Jeong and Neff [13], who then examined the stability, uniqueness and existence of the weakest possible constitutive equations. Bhattacharyya and Mukhopadhyay [14] modified the linear micropolar plate theory. The constitutive equations of inelastic micropolar materials were studied by Altenbach and Eremeyev [15]. Eremeyev and Konopińska-Zmysłowska [16] developed a unique definition of the local material symmetry group of micro-structures based on the strain and Kinetic energies of a micropolar medium with two kinematic fields.

Several works in the engineering literature have already described successful approaches to incorporate in-plane rotational DOF (also called drilling DOF) in membrane elements [17-20]. It is well known that increasing the drilling DOF at each node of a plane membrane element can improve element performance without increasing the element node numbers. As a nodal variable for interpolating element displacements, the drilling DOF was used in some studies [17]. In other works, a six-node triangular plane element or an eight-node quadrilateral element was transformed into a three-node or four-node element by substituting the middle side nodal displacements with the corner nodal displacements and rotations [18]. Hughes and Brezzi [19] presented a variational formulation by extending the skew-symmetric component of stress as a Lagrange multiplier. Ibrahimbegovic et al. [20] carried out a solution based on the hypothesis of Hughes and Brezzi [19] and the interpolation function of Allman [17]. Sangtarash et al. [21] developed an asymmetric quadrilateral membrane element with drilling DOF such that the required test functions are produced by enhancing four-node isoparametric-based displacement fields with drilling rotations. In such techniques, the drilling DOF is handled as a supplementary or internal variable.

Due to the mathematical complexity of higher-order continuum models, closed-form solutions are typically hard to find. In order to comprehend the materials at small scales and their complicated mechanical behavior, effective numerical approaches for micro-continuum field theories are needed. Finite Element Method (FEM) is a powerful numerical approach that works well for issues involving micro- and nanostructures. In this line, investigations focus on Cosserat theory's finite element formulations, including the research of Altenbach et al. [22], Yeh and Chen [23] and Huang et al. [24]. The theories of plates and shells based on Cosserat theory were introduced as unique applications of the theory of the micropolar continuum in [22]. It is worthwhile to mention that there is a body of work employing control volumes that is analogous to FEM to solve issues in micropolar elasticity [15]. Yeh and Chen [23] used Cosserat micropolar elasticity to create a degenerated shell element without spurious modes. Huang et al. [24] recognized the idea of enhancing the displacement field of standard FEM formulations in the framework of micropolar elasticity theory. Besides, Ansari et al. [25] developed a non-classical Three-Dimensional (3D) element based on the MPCT to examine the free vibration behavior of beam and plate-type structures. A size-dependent quadratic tetrahedral element was used by Kohansal-Vajargah and Ansari [26] to present the free vibration analysis of 3D micropolar structures with various geometries based on the 3D linear elasticity. Kohansal-Vajargah and Ansari [27] proposed a Two-Dimensional (2D) micropolar element to describe the free vibration behavior, in which the frequencies decreased as the micropolar effects became more dominant.

In this work, the non-dimensional natural frequency response of a novel size-dependent microplate element based on higher-order theory is studied using the finite element model. To do this, the element with drilling DOF is generally obtained for a higher-order plate theory utilizing a derived formulation based on the theory of Eringen's micropolar elasticity [6] before being matricized for computing purposes. After employing the minimum total potential energy principle, the mass and stiffness matrices of a size-dependent rectangular microplate with a suitable stiffness are developed. The length-scale parameter and micro-inertia affect the natural frequency response of micropolar plates. The devised quadratic size-dependent plate element, which contains the micro-rotation DOFs in addition to the translational ones of material particles, captures this influence. The suggested element is then used to examine the behavior of micropolar plates, while several numerical examples with the CCCC, SSSS, Clamped-Clamped (CC),

Clamped-Free (CF) and Simple-Free (SF) boundary conditions (free and clamped edges and simply supported are denoted by F, C and S, respectively) and various geometries corresponding to the length-scale parameter are simulated in the context of micropolar continuum mechanics to show the present work's applicability and validity. As examples of non-primitive geometry requiring irregular meshing, structures with a hole are used. According to certain researchers in [28], the presence of holes can also result in the structures being reinforced or weakened. Comparisons between the current calculated outcomes on the non-dimensional frequency of the natural oscillation of micropolar plates and their classical equivalent are done. This comprehensive study contributes to the understanding of the mechanical response of microplates, shedding light on the intricate interplay of micropolar effects, size-dependency, and geometric configurations.

2. Formulation of micropolar theory

Micropolar theory is considered as a micro-continuum theory that a rigid micro-structure is taken into account at each particle in which it is able to rotate independently from medium surrounding it. Thus, three classical translational DOFs and three rotational DOFs exist in this theory.

In Cartesian coordinate system, the tensor form of a micropolar continuum's governing equations of motion is formulated as [6,10].

$$\begin{aligned} &div(\tilde{\sigma})+\rho f=\rho\ddot{u}, \quad div(\tilde{\mu})+\rho m-\in:\sigma=\rho\, j\ddot{\phi},\\ &\sigma_{ij,j}+\rho f_i=\rho\ddot{u}, \quad u_{ij,j}+\rho m_i-\in_{ijk}\sigma_{jk}=\rho\, j\ddot{\phi}, \end{aligned} \tag{1}$$

in which ϕ and u represent the micro-rotation and displacement vectors, respectively; $\tilde{\mu}$ and $\tilde{\sigma}$ denote the couple stress tensor and the stress tensor, respectively; m and f stand for the body couple and the body force, respectively. Furthermore, $\in$ shows the permutation symbol. Also, the micro-inertia and mass density are denoted by j and ρ, respectively. Accordingly, in MPCT, the micro-strain tensors are characterized as [6]:

$$\tilde{\varepsilon}=Grad(\tilde{u})-\in\phi, \quad \tilde{\eta}=Grad(\phi), \tag{2}$$

in which indicial representations may be provided by:

$$\varepsilon_{ij}=u_{i,j}-\in_{ijk}\phi_k, \quad \eta_{ij}=\phi_{i,j}. \tag{3}$$

It is pointed out that the micro-strain tensors are asymmetric.

According to micropolar theory, the strain energy density $\widehat{W}$ can be characterized in the following form for the linear elastic micropolar element [10]:

$$\begin{aligned} \widehat{W}&=\frac{1}{2}\left(\begin{array}{c}\lambda tr^2\left(\tilde{\varepsilon}\right)+\left(\mu+\kappa\right)tr\left(\tilde{\varepsilon}\tilde{\varepsilon}^T\right)+\mu tr\left(\tilde{\varepsilon}^2\right)\\ +\alpha tr^2\left(\tilde{\eta}\right)+\beta tr\left(\tilde{\eta}^2\right)+\gamma tr\left(\tilde{\eta}\tilde{\eta}^T\right)\end{array}\right)\\ &=\frac{1}{2}\left(\begin{array}{c}\lambda\varepsilon_{ii}\varepsilon_{jj}+\left(\mu+\kappa\right)\varepsilon_{ij}\varepsilon_{ij}+\mu\varepsilon_{ij}\varepsilon_{ji}\\ +\alpha\eta_{ii}\eta_{jj}+\beta\eta_{ij}\eta_{ij}+\gamma\eta_{ij}\eta_{ji}\end{array}\right), \end{aligned} \tag{4}$$

where λ and μ denote the classical Lame coefficients, which are obtained as follows:

$$\begin{aligned} &\lambda=\frac{E\nu}{\left(1+\nu\right)\left(1-2\nu\right)}=\frac{2G\nu}{\left(1-2\nu\right)},\\ &2\mu+\kappa=2G=\frac{E}{\left(1+\nu\right)}. \end{aligned} \tag{5}$$

Also, α, β, γ, and κ are some of the material constants of micropolar [29] which are given by:

$$\begin{aligned} &\gamma=4Gl_b^2, \quad \mu=\frac{G\left(1-2N^2\right)}{1-N^2}, \quad \kappa=\frac{2GN^2}{1-N^2},\\ &\alpha=\left(4Gl_t^2\right)\left(\frac{1}{\psi}-1\right), \quad \beta=2G\left(l_t^2-2l_b^2\right). \end{aligned} \tag{6}$$

As a result, the stress and couple stress tensors for a linear elastic micropolar element are obtained using the strain energy density as follows:

$$\tilde{\sigma}=\frac{\partial\widehat{W}}{\partial\tilde{\varepsilon}}, \quad \tilde{\mu}=\frac{\partial\widehat{W}}{\partial\tilde{\eta}}. \tag{7}$$

Thus, MPCT's constitutive equations are expressed as [10]:

$$\tilde{\sigma}=\lambda tr\left(\tilde{e}\right)I+2\mu\tilde{e}+\kappa\tilde{\varepsilon}, \quad \tilde{\mu}=\alpha tr\left(\tilde{\eta}\right)+\beta\tilde{\eta}^T+\gamma\tilde{\eta}, \tag{8}$$

where I denotes the identity tensor and $\tilde{e}$ represents the classical strain that can be written as:

$$\tilde{e}=\frac{1}{2}\left(Grad\left(u\right)+Grad^T\left(u\right)\right). \tag{9}$$

The asymmetry of micro-strain tensors leads to asymmetric stress tensors of Eq. (8). In the Cartesian coordinate system, the components of stress and couple stress may be given as:

$$\sigma_{ij}=\lambda e_{kk}\delta_{ij}+2\mu e_{ij}+\kappa\varepsilon_{ij}, \qquad \mu_{ij}=\alpha\eta_{kk}\delta_{ij}+\beta\eta_{ji}+\gamma\eta_{ij}. \tag{10}$$

Utilizing the following relation [6]:

$$e_{ij}=\frac{1}{2}\left(\varepsilon_{ij}+\varepsilon_{ji}\right), \tag{11}$$

and defining two fourth-order tensors A_{ijkl} and $\overline{A}_{ijkl}$,

$$\begin{aligned} &A_{ijkl}=\lambda\delta_{ij}\delta_{kl}+\mu\left(\delta_{ik}\delta_{jl}+\delta_{il}\delta_{jk}\right)+\kappa\delta_{ik}\delta_{jl},\\ &\overline{A}_{ijkl}=\alpha\delta_{ij}\delta_{kl}+\beta\left(\delta_{il}\delta_{jk}\right)+\gamma\delta_{ik}\delta_{jl}, \end{aligned} \tag{12}$$

and by using Eqs. (10)-(12), the tensors of stress and couple stress can be restated as:

$$\sigma_{ij}=A_{ijkl}\varepsilon_{kl}, \quad \mu_{ij}=\overline{A}_{ijkl}\eta_{kl}. \tag{13}$$

By utilizing the preceding relations, the strain energy density's indicial form may be written as:

$$\widehat{W}=\frac{1}{2}\left(\sigma_{ij}\varepsilon_{ij}+\mu_{ij}\eta_{ij}\right)=\frac{1}{2}\left(A_{ijkl}\varepsilon_{ij}\varepsilon_{kl}+\overline{A}_{ijkl}\eta_{ij}\eta_{kl}\right). \tag{14}$$

From the computational point of view, Eq. (14) is considered as an important relation.

$$H=\begin{bmatrix}1&0&0&0&0&0&0&0&0\\0&0&0&0&1&0&0&0&0\\0&0&0&0&0&0&0&0&1\\0&0&0&0&0&1&0&0&0\\0&0&0&0&0&0&0&1&0\\0&0&0&0&0&0&1&0&0\\0&0&1&0&0&0&0&0&0\\0&1&0&0&0&0&0&0&0\\0&0&0&1&0&0&0&0&0\end{bmatrix},$$

$$q=\begin{bmatrix}U\\ \phi\end{bmatrix},\qquad U=\begin{bmatrix}u_1\\u_2\\u_3\end{bmatrix},\qquad \phi=\begin{bmatrix}\phi_1\\\phi_2\\\phi_3\end{bmatrix},\qquad P=\begin{bmatrix}0&0\\0&\overline{P}\end{bmatrix}_{9\times 6},\quad \overline{P}=I_3\otimes\begin{bmatrix}-1\\1\end{bmatrix}, \tag{19}$$

$$\theta=\begin{bmatrix}\frac{\partial u_1}{\partial x_1}&\frac{\partial u_2}{\partial x_1}&\frac{\partial u_3}{\partial x_1}&\frac{\partial u_1}{\partial x_2}&\frac{\partial u_2}{\partial x_2}&\frac{\partial u_3}{\partial x_2}&\frac{\partial u_1}{\partial x_3}&\frac{\partial u_2}{\partial x_3}&\frac{\partial u_3}{\partial x_3}\end{bmatrix}^T,$$

$$\overline{\theta}=\begin{bmatrix}\frac{\partial \phi_1}{\partial x_1}&\frac{\partial \phi_2}{\partial x_1}&\frac{\partial \phi_3}{\partial x_1}&\frac{\partial \phi_1}{\partial x_2}&\frac{\partial \phi_2}{\partial x_2}&\frac{\partial \phi_3}{\partial x_2}&\frac{\partial \phi_1}{\partial x_3}&\frac{\partial \phi_2}{\partial x_3}&\frac{\partial \phi_3}{\partial x_3}\end{bmatrix}^T.$$

Box I

Multiplication of matrices can be used to get the indicial form of the strain energy density.

The material position vector may be defined as follows [30]:

$$u_i\left(\xi_1,\xi_2,\xi_3\right)=u_{0_i}\left(\xi_1,\xi_2\right)+\frac{h}{2}\xi_3 e_{ijk}\phi_j\left(\xi_1,\xi_2\right)n_k\left(\xi_1,\xi_2\right), \tag{15}$$

where $\left(\xi_1,\xi_2\right)$ denotes the non-dimensional coordinates in the plane of the plate, and ξ_3 denotes the non-dimensional coordinate in the thickness direction ($-1\prec\xi_3\prec 1$ through the thickness). The coordinates of the reference surface are given by $u_{0_i}\left(\xi_1,\xi_2\right)$ at the nodes. As regards, $n_1=n_2=0$, $n_3=1$ are on the x_1-x_2 plane.

In this perspective, the components of $\tilde{\varepsilon}$ and $\tilde{\eta}$ are arranged within the following matrice forms:

$$\tilde{\varepsilon}=\begin{bmatrix}\varepsilon_{11}&\varepsilon_{12}&\varepsilon_{13}\\\varepsilon_{21}&\varepsilon_{22}&\varepsilon_{23}\\\varepsilon_{31}&\varepsilon_{32}&\varepsilon_{33}\end{bmatrix},\quad \tilde{\eta}=\begin{bmatrix}\eta_{11}&\eta_{12}&\eta_{13}\\\eta_{21}&\eta_{22}&\eta_{23}\\\eta_{31}&\eta_{32}&\eta_{33}\end{bmatrix}, \tag{16}$$

and one can introduce the following vectors:

$$\varepsilon=\varepsilon_o+\frac{h}{2}\xi_3\varepsilon_b,$$
$$\varepsilon_o=\begin{bmatrix}\varepsilon_{o11}&\varepsilon_{o22}&\varepsilon_{o33}&\varepsilon_{o23}&\varepsilon_{o32}&\varepsilon_{o31}&\varepsilon_{o13}&\varepsilon_{o12}&\varepsilon_{o21}\end{bmatrix}^T,$$
$$\varepsilon_b=\begin{bmatrix}\varepsilon_{b11}&\varepsilon_{b22}&\varepsilon_{b33}&\varepsilon_{b23}&\varepsilon_{b32}&\varepsilon_{b31}&\varepsilon_{b13}&\varepsilon_{b12}&\varepsilon_{b21}\end{bmatrix}^T, \tag{17}$$
$$\eta=\begin{bmatrix}\eta_{11}&\eta_{22}&\eta_{33}&\eta_{23}&\eta_{32}&\eta_{31}&\eta_{13}&\eta_{12}&\eta_{21}\end{bmatrix}^T,$$

or,

$$\varepsilon=H\theta+Pq,\quad \eta=H\overline{\theta}, \tag{18}$$

where the details of Eq. (18) are shown in Eq. (19) in Box I, as I_3 shows the three-by-three identity matrix and $\otimes$ represents the Kronecker product symbol.

The relationship between lengths dx_1, dx_2, dx_3 in x_1, x_2, x_3 space and $d\xi_1$, $d\xi_2$, $d\xi_3$ in ξ_1, ξ_2, ξ_3 space can be rewritten as follows:

$$\begin{bmatrix}dx_1\\dx_2\\dx_3\end{bmatrix}=\left[J\right]\begin{bmatrix}d\xi_1\\d\xi_2\\d\xi_3\end{bmatrix}, \tag{20}$$

wherein:

$$\left[J\right]=\begin{bmatrix}\frac{dx_1}{d\xi_1}&\frac{dx_1}{d\xi_2}&\frac{dx_1}{d\xi_2}\\\frac{dx_2}{d\xi_1}&\frac{dx_2}{d\xi_2}&\frac{dx_2}{d\xi_3}\\\frac{dx_3}{d\xi_1}&\frac{dx_3}{d\xi_2}&\frac{dx_3}{d\xi_3}\end{bmatrix}. \tag{21}$$

The asymmetric bending and transverse shear strains are substituted with half of their corresponding engineering strains in order to preserve the drilling DOF and avoid using engineering strains. The bending strains also disappear in the transverse direction [23]. Consequently, the strain vector $\hat{\varepsilon}$ of a general plate is rewritten as:

$$\hat{\varepsilon}=\hat{\varepsilon}_0+\frac{h}{2}\xi_3\hat{\varepsilon}_b \tag{22}$$

where Eq. (23) is shown in Box II.

$$\hat{\varepsilon}_0 = \left[\begin{array}{ccccccccc} \varepsilon_{o11} & \varepsilon_{o22} & \varepsilon_{o33} & \frac{1}{2}(\varepsilon_{o23}+\varepsilon_{o32}) & \frac{1}{2}(\varepsilon_{o23}+\varepsilon_{o32}) & \frac{1}{2}(\varepsilon_{o31}+\varepsilon_{o13}) & \frac{1}{2}(\varepsilon_{o31}+\varepsilon_{o13}) & \varepsilon_{o12} & \varepsilon_{o21} \end{array}\right]^T,$$
$$\hat{\varepsilon}_b = \left[\begin{array}{ccccccccc} \varepsilon_{b11} & \varepsilon_{b22} & \varepsilon_{b33} & \varepsilon_{b23} & \varepsilon_{b32} & \varepsilon_{b31} & \varepsilon_{b13} & \frac{1}{2}(\varepsilon_{b12}+\varepsilon_{b21}) & \frac{1}{2}(\varepsilon_{b12}+\varepsilon_{b21}) \end{array}\right]^T. \quad (23)$$

Box II

$$A = \begin{bmatrix} \lambda_1+2\mu+\kappa & \lambda_1 & 0 & 0 & 0 & 0 & 0 & 0 & 0 \\ & \lambda_1+2\mu+\kappa & 0 & 0 & 0 & 0 & 0 & 0 & 0 \\ & & 0 & 0 & 0 & 0 & 0 & 0 & 0 \\ & & & k_s(\mu+\kappa) & k_s\mu & 0 & 0 & 0 & 0 \\ & & & & k_s(\mu+\kappa) & 0 & 0 & 0 & 0 \\ & & & & & k_s(\mu+\kappa) & k_s\mu & 0 & 0 \\ & & Sym. & & & & k_s(\mu+\kappa) & 0 & 0 \\ & & & & & & & \mu+\kappa & \mu \\ & & & & & & & & \mu+\kappa \end{bmatrix},$$

$$\bar{A} = \begin{bmatrix} \lambda_2+\beta+\gamma & \lambda_2 & 0 & 0 & 0 & 0 & 0 & 0 & 0 \\ & \lambda_2+\beta+\gamma & 0 & 0 & 0 & 0 & 0 & 0 & 0 \\ & & 0 & 0 & 0 & 0 & 0 & 0 & 0 \\ & & & \gamma & \beta & 0 & 0 & 0 & 0 \\ & & & & \gamma & 0 & 0 & 0 & 0 \\ & & & & & \gamma & \beta & 0 & 0 \\ & & Sym. & & & & \gamma & 0 & 0 \\ & & & & & & & \gamma & \beta \\ & & & & & & & & \gamma \end{bmatrix}. \quad (27)$$

Box III

Moreover, the stress and couple stress vectors may be considered as follows:

$$\sigma = \left[\sigma_{11} \quad \sigma_{22} \quad \sigma_{33} \quad \sigma_{23} \quad \sigma_{32} \quad \sigma_{31} \quad \sigma_{13} \quad \sigma_{12} \quad \sigma_{21}\right]^T,$$
$$\mu = \left[\mu_{11} \quad \mu_{22} \quad \mu_{33} \quad \mu_{23} \quad \mu_{32} \quad \mu_{31} \quad \mu_{13} \quad \mu_{12} \quad \mu_{21}\right]^T. \quad (24)$$

Thus, for a linear micropolar elasticity continuum, the formulation of the constitutive equation is expressed as follows:

$$\sigma = A\hat{\varepsilon}, \quad \mu = \bar{A}\eta, \quad (25)$$

in which A and $\bar{A}$ denote the symmetric forms of the micropolar elastic stiffness matrices, which are written as:

$$A = \begin{bmatrix} A_{1111} & A_{1122} & A_{1133} & A_{1123} & A_{1132} & A_{1131} & A_{1113} & A_{1112} & A_{1121} \\ & A_{2222} & A_{2233} & A_{2223} & A_{2232} & A_{2231} & A_{2213} & A_{2212} & A_{2221} \\ & & A_{3333} & A_{3323} & A_{3332} & A_{3331} & A_{3313} & A_{3312} & A_{3321} \\ & & & A_{2323} & A_{2332} & A_{2331} & A_{2313} & A_{2312} & A_{2321} \\ & & & & A_{3232} & A_{3231} & A_{3213} & A_{3212} & A_{3221} \\ & & & & & A_{3131} & A_{3113} & A_{3112} & A_{3121} \\ & & Sym. & & & & A_{1313} & A_{1312} & A_{1321} \\ & & & & & & & A_{1212} & A_{1221} \\ & & & & & & & & A_{2121} \end{bmatrix}_{9\times 9}$$

$$\bar{A} = \begin{bmatrix} \bar{A}_{1111} & \bar{A}_{1122} & \bar{A}_{1133} & \bar{A}_{1123} & \bar{A}_{1132} & \bar{A}_{1131} & \bar{A}_{1113} & \bar{A}_{1112} & \bar{A}_{1121} \\ & \bar{A}_{2222} & \bar{A}_{2233} & \bar{A}_{2223} & \bar{A}_{2232} & \bar{A}_{2231} & \bar{A}_{2213} & \bar{A}_{2212} & \bar{A}_{2221} \\ & & \bar{A}_{3333} & \bar{A}_{3323} & \bar{A}_{3332} & \bar{A}_{3331} & \bar{A}_{3313} & \bar{A}_{3312} & \bar{A}_{3321} \\ & & & \bar{A}_{2323} & \bar{A}_{2332} & \bar{A}_{2331} & \bar{A}_{2313} & \bar{A}_{2312} & \bar{A}_{2321} \\ & & & & \bar{A}_{3232} & \bar{A}_{3231} & \bar{A}_{3213} & \bar{A}_{3212} & \bar{A}_{3221} \\ & & & & & \bar{A}_{3131} & \bar{A}_{3113} & \bar{A}_{3112} & \bar{A}_{3121} \\ & & Sym. & & & & \bar{A}_{1313} & \bar{A}_{1312} & \bar{A}_{1321} \\ & & & & & & & \bar{A}_{1212} & \bar{A}_{1221} \\ & & & & & & & & \bar{A}_{2121} \end{bmatrix}_{9\times 9} \quad (26)$$

Using Eq. (12), with considering k_s as the shear correction factor, A and $\bar{A}$ obtained by Eq. (27) is shown in Box III, in which:

$$\lambda_1 = \lambda\left(1-\frac{\lambda}{\lambda+2\mu+\kappa}\right), \quad \lambda_2 = \alpha\left(1-\frac{\alpha}{\alpha+\beta+\gamma}\right). \quad (28)$$

Therefore, the relation of the strain energy density of Eq. (14) is restated as:

$$\widehat{W} = \frac{1}{2}\left(\varepsilon^T\sigma+\eta^T\mu\right) = \frac{1}{2}\left(\varepsilon^T A\varepsilon+\eta^T\bar{A}\eta\right). \quad (29)$$

By introducing C and γ as the elastic stiffness matrix and

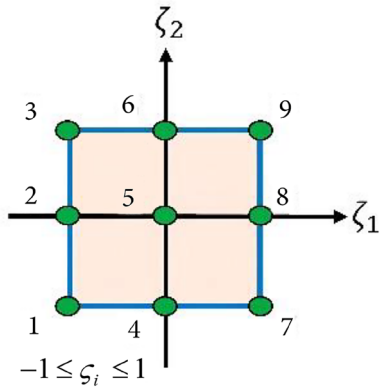

$$d^i(\varsigma)=\left[u_1^i(\varsigma)\ u_2^i(\varsigma)\ u_3^i(\varsigma)\quad i=1,2 \right.$$
$$\left.\phi_1^i(\varsigma)\ \phi_2^i(\varsigma)\ \phi_3^i(\varsigma)\right]^T \quad i=1,\ldots,i_{\max}$$

Figure 1. Rectangular micropolar plate element.

micro-strain vector, respectively, one can rewrite the elastic strain energy density relation as follows:

$$\widehat{W}=\frac{1}{2}\gamma^T C\gamma, \tag{30}$$

wherein,

$$\gamma=\begin{bmatrix}\hat{\varepsilon}\\ \eta\end{bmatrix},\quad C=\begin{bmatrix}A & 0\\ 0 & \overline{A}\end{bmatrix}. \tag{31}$$

Finally, the strain and Kinetic energies may be calculated as follows, respectively:

$$\begin{aligned} W&=\frac{1}{2}\int_V \widehat{W}dV=\frac{1}{2}\int_V \gamma^T C\gamma dV,\\ T&=\frac{1}{2}\int_V\left(\rho\dot{u}_i\dot{u}_i+\rho j\dot{\phi}_i\dot{\phi}_i\right)dV, \end{aligned} \tag{32}$$

and the corresponding variational forms of the Kinetic and strain energies can be expressed as:

$$\begin{aligned} \delta W&=\int_V \delta\gamma^T C\gamma dV,\\ \delta T&=\frac{1}{2}\int_V\left(\rho\delta u_i\ddot{u}_i+\rho j\delta\phi_i\ddot{\phi}_i\right)dV. \end{aligned} \tag{33}$$

By integrating from t_1 to t_2 one obtains:

$$\int_{t_1}^{t_2}\delta T dt=-\int_{t_1}^{t_2}\int_V\left(\rho\delta u^T\ddot{u}+\rho j\delta\phi^T\ddot{\phi}\right)dV, \tag{34}$$

where t stands for time.

One can write the variational equation of motion using the Hamilton's principle as:

$$\delta\int_{t_1}^{t_2}(T-W)dt=0. \tag{35}$$

3. Formulation of micropolar finite elements

Figure 1 shows the suggested schematic for a rectangular micropolar plate element. It introduces a quadratic element with nine nodes. The suggested element has six DOFs at each node. There are three DOFs for translation and three DOFs for rotation.

Consequently, the element's micro-strain vector is obtained in the manner shown below:

$$\gamma_e=Bd. \tag{36}$$

As a result, an element's strain energy density is given as:

$$\widehat{W}_e=\frac{1}{2}d^T B^T CBd. \tag{37}$$

The strain energy is obtained as follows by substituting Eq. (37) into Eq. (32).

$$W_e=\frac{1}{2}d^T\int_{V_e}B^T CBdVd=\frac{1}{2}d^T Kd,\quad K=\int_{V_e}B^T CBdV, \tag{38}$$

where K denotes the stiffness matrix.

In the end, by utilizing the Hamilton's principle given in Eq. (35), the governing equations for free vibration are found as below:

$$M\ddot{d}+Kd=0,\quad \ddot{d}=-\omega^2 d \tag{39}$$

where ω represents the natural frequency.

Table 1. Comparison between the results of a microbeam.

H (in)	Current work (in)	Theoretical solution (in) [24]	Numerical solution (in) [24]
0.2	0.2617	0.2614	0.2669
0.4	0.03403	0.03380	0.03412

4. Validation study

The analysis of a microbeam is carried out first, and the results are compared with the results of the study of Huang et al. [24] to guarantee the correctness and validity of the current study and the developed micropolar plate element.

Table 1 presents a comparison of the deflection values for a microbeam under identical loading conditions, geometrical data, and material constants. The table includes results from the current study, a theoretical solution, and a numerical solution referenced from [24]. The deflection values are provided for different cross-section heights (H). The purpose of the table is to demonstrate the agreement between the deflection results obtained in the current work and those reported in the literature. Investigations are also done on the relationship between the deflection of a micropolar beam and the value of γ. Figure 2 displays a comparison between the outcomes and those mentioned in [24].

In the next case, the article by Sargsyan and Sargsyan [7] is taken into consideration in the context of micropolar plates, where the frequencies of natural oscillations of square microplates with simply-supported boundary condition are given using comparable hypotheses. Results are presented in Figure 3 according to adopting notations (α, β, $\in$ and γ are

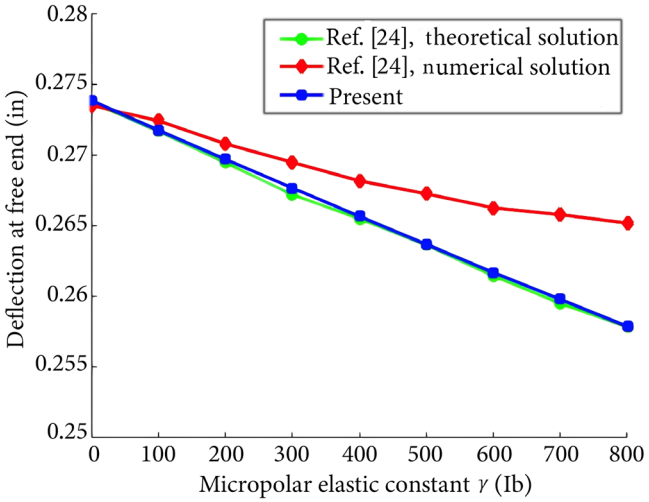

Figure 2. Relation of deflection against value of for the microbeam.

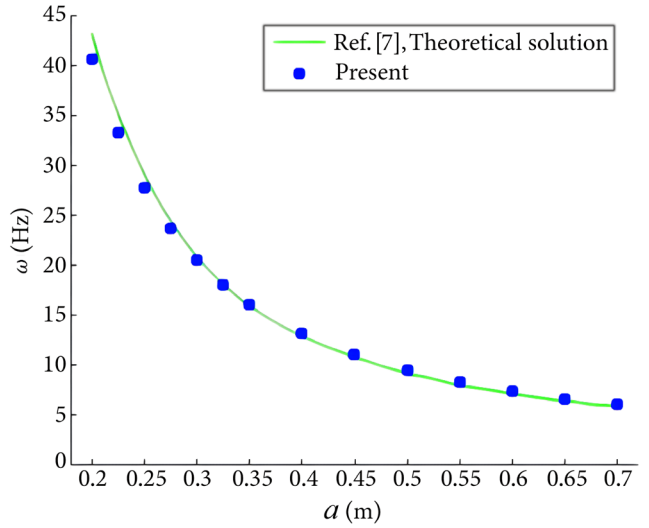

Figure 3. Comparison of lowest frequency of natural oscillation of the square microplate on its size $0.2 \le \alpha \le 0.7$, predicted in [7] and present work ($\frac{h}{2a} = \frac{1}{40}$).

instead of κ, α, β and γ, respectively). Moreover, the frequencies of higher-order microplate shown here agree well with the theoretical solutions of the literature.

5. Frequencies of natural oscillations of microplates with various geometries

Here, the natural frequencies of microplates with diverse geometries are examined using the proposed 9-nod quadrilateral micropolar element. Square microplates with and without a central hole, and a circular microplate with a central hole are three different types of geometry that are taken into account. The parameters mentioned below are defined as:

$$\Omega = L^2\omega\sqrt{\frac{\rho h}{D}}, \quad D = \frac{(\lambda + 2\mu + \kappa)h^3}{12},$$

where Ω is the non-dimensional frequency of natural oscillation of the micropolar plate. The constants listed in Table 2 are used to calculate the frequencies' values.

Table 2. Properties of the microplate [29].

Parameter	Definition	Value
Young's modulus (MPa)	$E = \frac{(2\mu+\kappa)(3\lambda+2\mu+\kappa)}{2\lambda+2\mu+\kappa}$	299.52
Shear modulus (MPa)	$G = \frac{2\mu+\kappa}{2}$	104
Poisson's ratio	$\nu = \frac{\lambda}{2\lambda+2\mu+\kappa}$	0.44
Coupling number	$N^2 = \frac{\kappa}{2(\mu+\kappa)}$	0.04
Characteristic length (bending) (mm)	$l_b = \sqrt{\frac{\gamma}{2(2\mu+\kappa)}}$	0.33
Characteristic length (torsion) (mm)	$l_t = \sqrt{\frac{\beta+\gamma}{\alpha+\beta+\gamma}}$	0.62
Polar ratio	$\psi = \frac{\beta+\gamma}{\alpha+\beta+\gamma}$	1.5
Density (N/mm^3)	ρ	2e-9
Micro-inertia (mm^2)	j	50

Table 3. Convergence study of the first five frequencies of natural oscillations (kHz) of the microplate (CCCC, $\frac{h}{l_b} = 10$; $\frac{L}{h} = 10$).

Number of elements	ω_1	ω_2	ω_3	ω_4	ω_5
6 × 6	1.5034	2.3187	2.3187	2.8504	3.1690
8 × 8	1.5032	2.3158	2.3158	2.8485	3.1563
10 × 10	**1.5031**	2.3149	2.3149	2.8480	3.1524
12 × 12	**1.5031**	2.3146	2.3146	2.8478	3.1509
14 × 14	**1.5031**	2.3145	2.3145	2.8477	3.1503
16 × 16	**1.5031**	**2.3144**	**2.3144**	**2.8476**	3.1499
18 × 18	**1.5031**	**2.3144**	**2.3144**	**2.8476**	3.1497
20 × 20	**1.5031**	**2.3144**	**2.3144**	**2.8476**	**3.1496**
22 × 22	**1.5031**	**2.3144**	**2.3144**	**2.8476**	**3.1496**

The bold shows the converged value.

5.1. Example 1: Frequencies of natural oscillations of the square microplate

For a microplate with $\frac{L}{h} = 10$, the length scale parameter effects (l_b) on the first five non-dimensional frequencies of natural oscillations are examined in this section. Here, L and h represent the length and thickness of the side, respectively. The CCCC and SSSS boundary conditions are applied to the microplates. Additionally, the effects of geometry on the frequencies of natural oscillations of micropolar plates are reviewed.

In order to do this, Table 3 provides the first five frequencies of natural oscillations of the square microplate for various elements number, with $\frac{h}{l_b} = 10$ an $\frac{L}{h} = 10$. The convergence behavior of the proposed approach improves as the elements number increases, as seen in Table 3. It was concluded that the use of higher-order plate theory tends to converge the frequencies of microplates with fewer elements compared to the literature. Specifically, the first five natural frequencies in the present work converge with a computational model consisting of 400 elements, 1681 nodes,

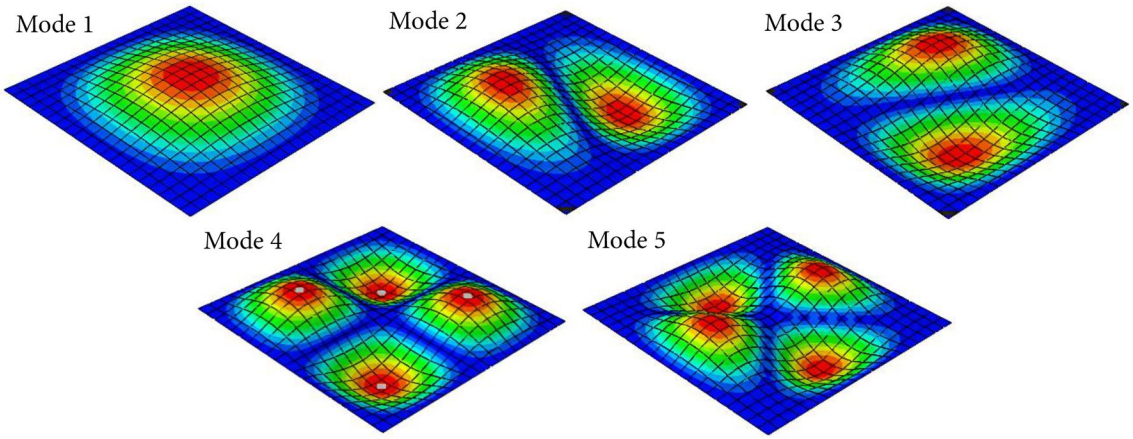

Figure 4. Mode shapes of CCCC square microplate.

Table 4. First five frequencies of natural oscillations (kHz) of a square microplate (CCCC, $h/l_b = 10$; $L/h = 10$).

Frequency	CT-ABAQUS	CT-present	MPT
ω_1	1.9125	1.9100	1.5031
ω_2	3.6107	3.6038	2.3144
ω_3	3.6107	3.6038	2.3144
ω_4	5.0290	5.0175	2.8476
ω_5	5.9002	5.8851	3.1496

and 10086 DOFs, while the convergence in Ref. [26] is achieved with a model comprising 5400 elements, more than 8904 nodes, and more than 53424 DOFs. This emphasizes the efficiency and computational advantages of the developed plate element in this study.

The results of the comparison between the first five frequencies of natural oscillations of a square microplate and corresponding frequencies of natural oscillations of the classical theory are shown in Table 4. The CT frequencies and those obtained using the commercial software ABAQUS are quite consistent. According to the frequency values in this table, the micro-inertia has a significant effect and diminishes the stiffness of microplate in the free vibration analysis. Figure 4 displays the CCCC square microplate's first five mode shapes.

The relationship between the thickness-to-length scale ratio ($\frac{h}{l_b}$) and the square micropolar plate's first five non-dimensional frequencies is illustrated in Figure 5. Additionally, for comparison, Figure 5 shows the expected non-dimensional classical frequencies of natural oscillations. It is important to note that during the computations a fixed length scale parameter (l_b) should be used, similar to the material characteristics. This figure illustrates how the effects captured by MPCT and the distinction between the corresponding micropolar and classical frequencies are significant at the small values of $\frac{h}{l_b}$. This figure also shows that the distinction between the frequencies of natural oscillations expected by the micro-

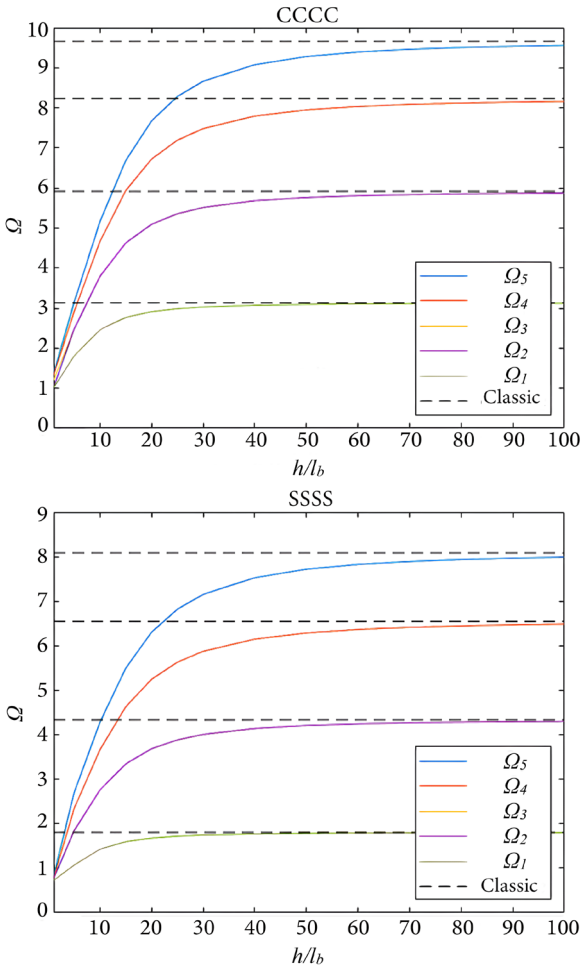

Figure 5. Non-dimensional natural frequencies of rectangular microplate discrepancy versus thickness-to-length scale ratio ($\frac{L}{h} = 10$).

polar theory and classical theory may be omitted for larger values of $\frac{h}{l_b}$. As a result, it was shown that higher modes had a larger effect on material characteristics. When the microplate's value of the thickness is small ($h = l_b$), it is noticed that the discrepancy between MPCT and CT frequencies at higher modes is larger than the frequency values at lower modes.

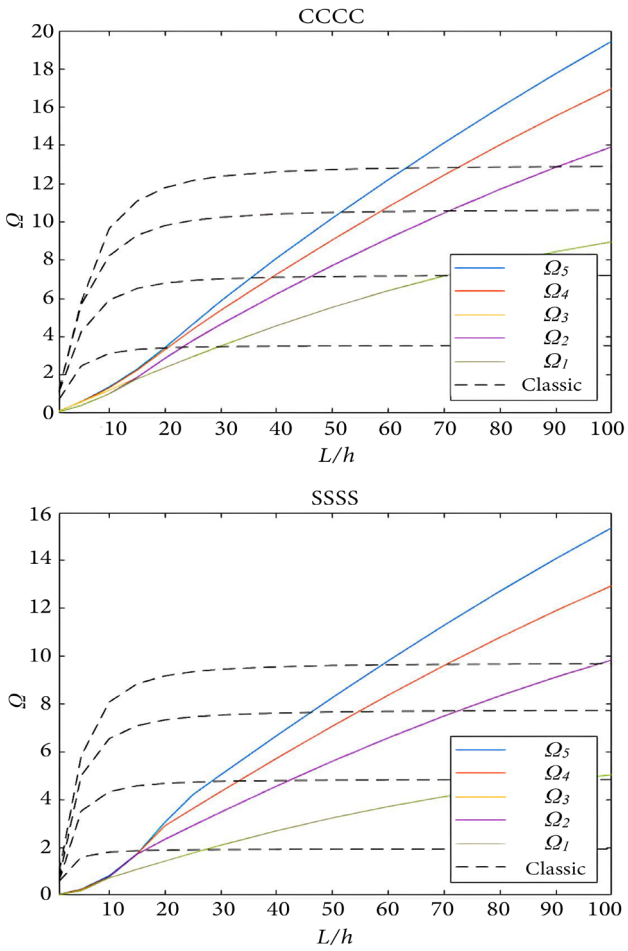

Figure 6. Non-dimensional natural frequencies of rectangular microplate discrepancy versus length-to-thickness ratio ($\frac{h}{l_b} = 1$).

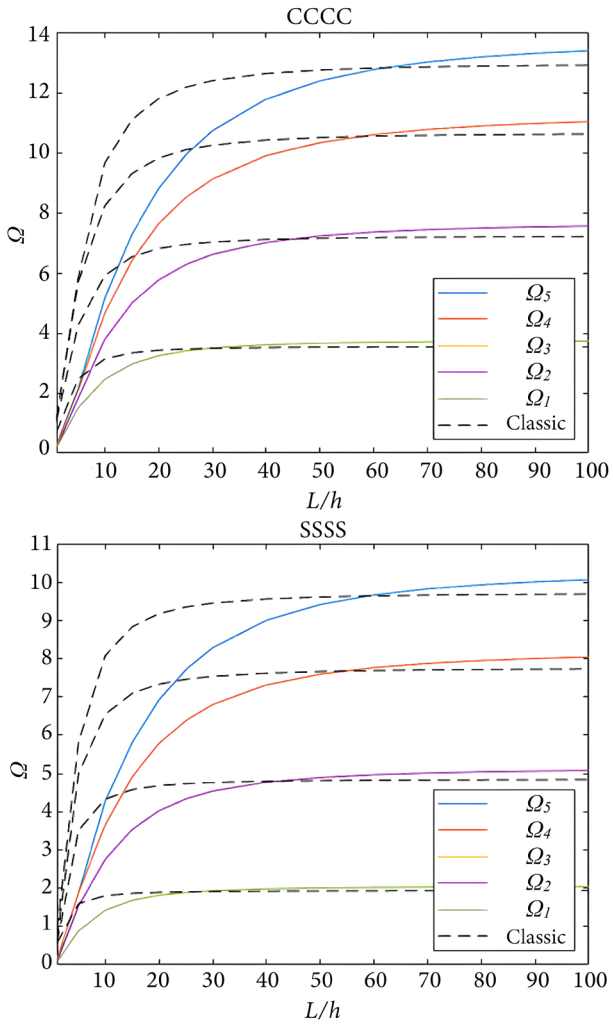

Figure 7. Non-dimensional natural frequencies of rectangular microplate discrepancy versus length-to-thickness ratio $\frac{(h}{l_b} = 10$).

In addition, Figures 6 and 7 illustrate how the side-to-thickness ratio ($\frac{L}{h}$) affects the frequencies of natural oscillations of microplates with $\frac{h}{l_b} = 1$ and $\frac{h}{l_b} = 10$, respectively. Additionally, these figures include the values of the respective classical frequencies. The values of frequencies of natural oscillations in different modes demonstrated here increase by increasing the $\frac{L}{h}$ ratio. The size effects on the characteristics of material discovered here are significant for large values of $\frac{L}{h}$ and increase the stiffness of the square plate.

5.2. Example 2: Frequencies of natural oscillations of the annular microplate

The vibration behavior of an annular microplate with CC, CF and SF boundary conditions is investigated in the next case. R_i and R_o are the inner and outer radius of an annular microplate, respectively. Also, it is assumed that $R_o = 2R_i$ and $l = R_o - R_i$. The first five frequencies of natural oscillations of the annular microplate for various elements number, with $\frac{h}{l_b=10}$ and $\frac{l}{h=10}$, are provided in Table 5.

The comparison between the first five frequencies of natural oscillations of an annular micropolar plate and the CT is presented in Table 6. Like in the preceding example, the effect of micro-inertia in this example is considerable. It has been shown that micropolarity reduces the plate stiffness,

Table 5. Convergence study of the first five frequencies of natural oscillations (kHz) of an annular microplate ($CC, h/l_b = 10$; $l/h = 10$).

Number of elements	ω_1	ω_2	ω_3	ω_4	ω_5
32	1.0900	1.0942	1.0942	1.1072	1.1109
50	1.0875	1.0915	1.0915	1.1038	1.1074
72	1.0866	1.0904	1.0904	1.1025	1.1061
98	1.0862	1.0900	1.0900	1.1020	1.1056
128	1.0860	1.0898	1.0898	1.1017	1.1053
162	1.0859	1.0897	1.0897	1.1016	1.1052
200	**1.0858**	1.0896	1.0896	1.1015	1.1051
242	**1.0858**	**1.0895**	**1.0895**	**1.1014**	**1.1050**
288	**1.0858**	**1.0895**	**1.0895**	**1.1014**	**1.1050**

The bold shows the converged value.

Table 6. First five frequencies (kHz) of an annular microplate. ($CC, h/l_b = 10$; $l/h = 10$).

Frequency	CT-ABAQUS	CT-present	MPCT
ω_1	1.2283	1.2266	1.0858
ω_2	1.2405	1.2388	1.0895
ω_3	1.2405	1.2388	1.0895
ω_4	1.2795	1.2779	1.1014
ω_5	1.2795	1.2779	1.1050

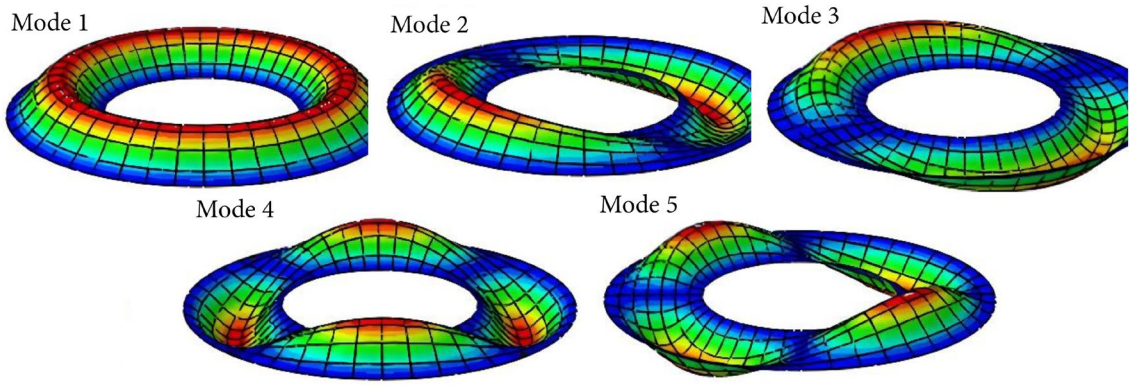

Figure 8. Mode shapes of CC annular microplate.

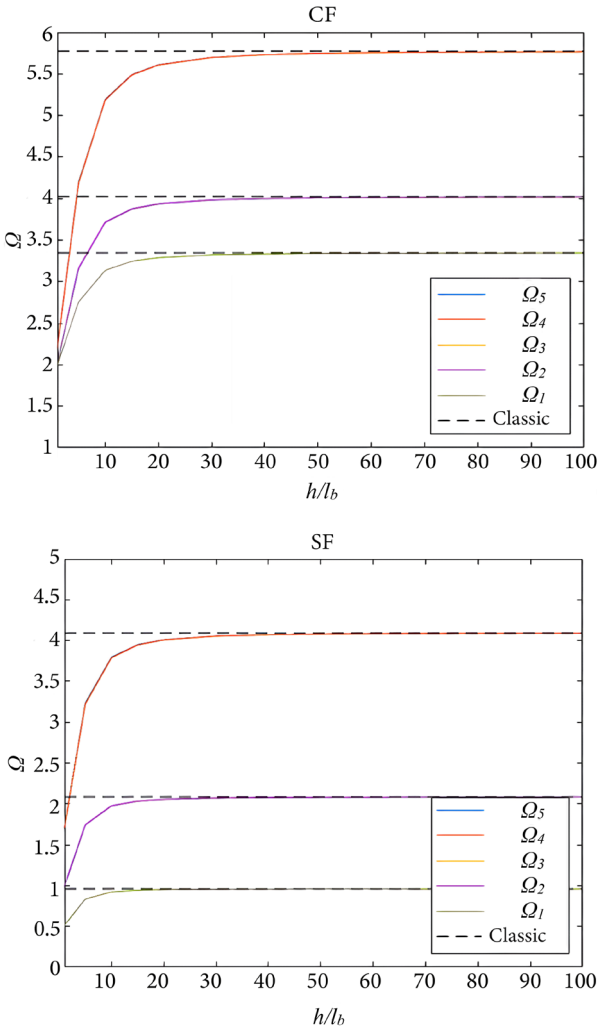

Figure 9. Non-dimensional natural frequencies of annular microplate discrepancy versus thickness-to-length scale ratio ($\frac{l}{h} = 10$).

which in turn reduces the frequencies of natural oscillations' values of microplate, and are smaller than classical frequencies. Figure 8 displays the annular structure's first five mode shapes.

Figure 9 illustrates the first five non-dimensional frequencies within the annular microplate which are under the effect of length scale parameter. The results shown here

Table 7. Convergence study of the first five frequencies of natural oscillations (kHz) of the microplate (CC, $h/l_b = 10$; $L/h = 10$).

Number of elements	ω_1	ω_2	ω_3	ω_4	ω_5
128	4.8254	4.8254	4.8387	4.8530	4.9588
288	4.8210	4.8210	4.8324	4.8447	4.9529
512	**4.8200**	**4.8200**	**4.8303**	**4.8432**	**4.9501**
800	**4.8200**	**4.8200**	**4.8303**	**4.8429**	**4.9490**

The bold shows the converged value.

are aimed to represent the influences of the length scale parameter (l_b) and material characteristics on the vibrational behavior of the micropolar annular plate. One can observe that the small-scaled micropolar plates' frequencies of natural oscillations are overestimated by the classical elasticity. Moreover, the convergence to classical results occurs at higher modes and larger values of $\frac{h}{l_b}$. Figures 10 and 11 clearly show the considerable effects of the boundary conditions and length-to-thickness ratio ($\frac{l}{h}$) on the frequencies of natural oscillations of the annular microplate. It is demonstrated that distinct mode frequencies increase when the value of $\frac{l}{h}$ increases, particularly from $\frac{l}{h} = 1$ to $\frac{l}{h} = 20$.

5.3. *Example 3: Frequencies of natural oscillations of the square microplate with a central hole*

The next case focuses on investigating the influence of micropolarity on the vibrational characteristics of a specific geometric configuration: A square microplate with a central hole. The obtained results were then compared with the frequencies of micropolar square plates that do not feature a central hole. The CC, CF, and SF boundary conditions are applied to the plates that include a central hole. The dimensions of the central hole are defined relative to the length of the side of the square microplate, with the outer length being twice the inner length. L represents the outer length of a square micropolar plate with a central hole.

Table 7 presents the first five frequencies of natural oscillations for a square microplate, considering various

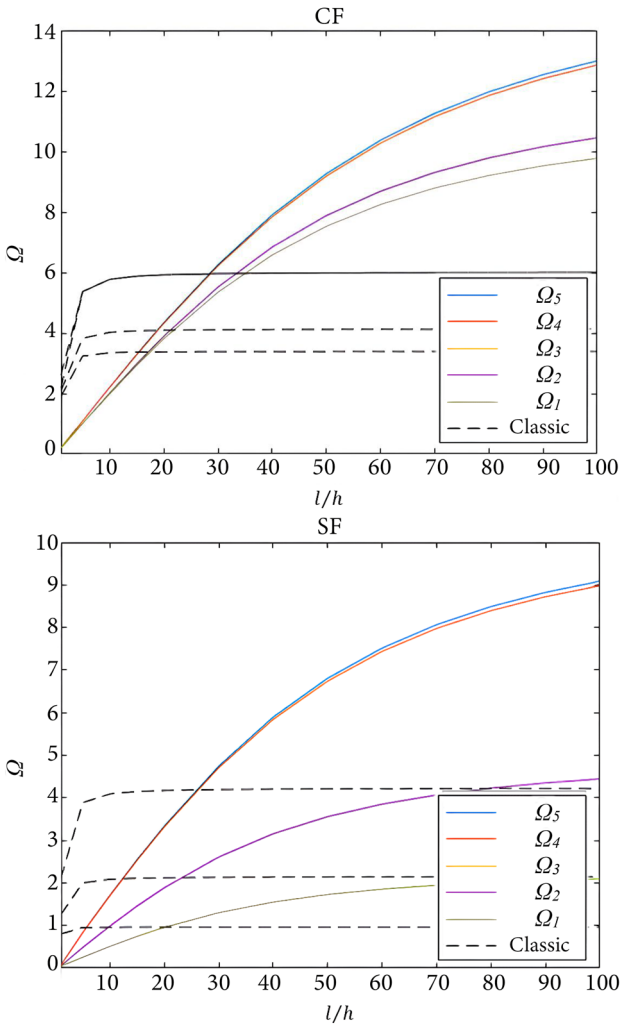

Figure 10. Non-dimensional natural frequencies of annular microplate discrepancy versus length-to-thickness ratio ($\frac{h}{l_b}=1$).

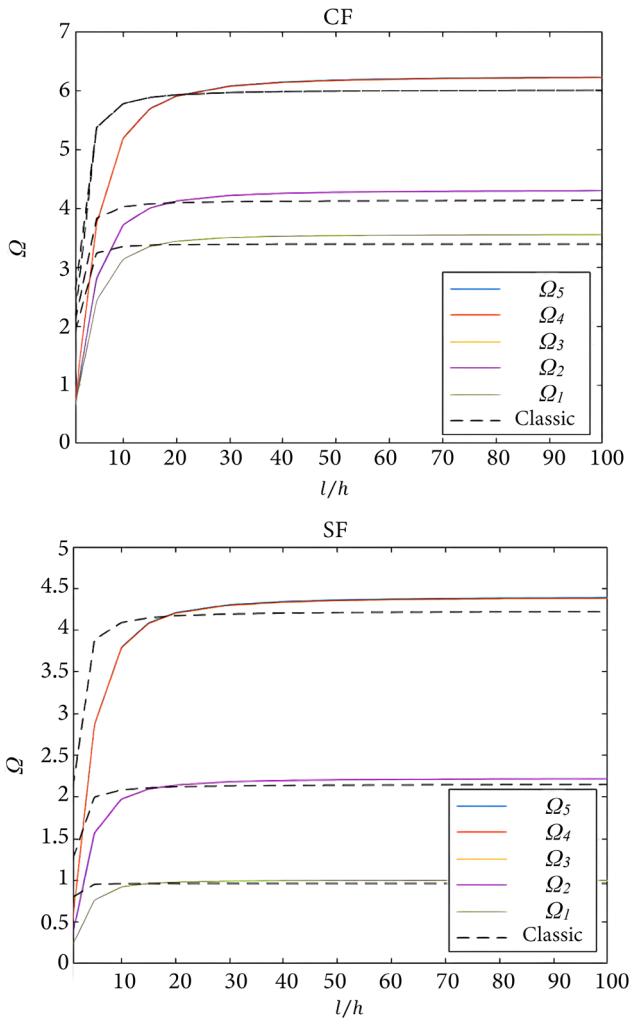

Figure11. Non-dimensional natural frequencies of annular microplate discrepancy versus length-to-thickness ratio ($\frac{h}{l_b}=10$).

Table 8. First five frequencies of natural oscillations (kHz) of a square microplate with a central hole (CC, $h/l_b=10$; $L/h=10$).

Frequency	CT-ABAQUS	CT-present	MPCT
ω_1	10.005	9.9479	4.8200
ω_2	10.010	9.9555	4.8200
ω_3	10.010	9.9555	4.8303
ω_4	10.017	9.9622	4.8429
ω_5	11.114	10.6531	4.9490

element numbers, with $\frac{h}{l_b}=10$ and $\frac{L}{h}=10$. The convergence behavior of the proposed approach improves as the number of elements increases, as observed in Table 7.

The results of the comparison between the first five frequencies of natural oscillations of a square microplate with a central hole and the corresponding frequencies of natural oscillations from classical theory are presented in Table 8. Similar to the preceding examples, the frequencies from the CT and those obtained using the ABAQUS show consistent results. The table indicates that micro-inertia has a significant effect, reducing the stiffness of the micropolar plate in free vibration analysis. Consequently, the frequencies of natural oscillations for the microplate are smaller than classical frequencies. Figure 12 displays the first five mode shapes of the CC square microplate structure.

The relationship between the thickness-to-length scale ratio ($\frac{h}{l_b}$) and the first five non-dimensional frequencies of the square microplate with a central hole is illustrated in Figure 13. The figure also includes the expected non-dimensional classical frequencies of natural oscillations for comparison. It's essential to note that a fixed length scale parameter (l_b) is maintained during the computations, similar to the material characteristics. The figure demonstrates the significant effects captured by MPCT and the notable distinction between micropolar and classical frequencies, particularly at small values of $\frac{h}{l_b}$. Moreover, the figure indicates that as $\frac{h}{l_b}$ increases, the difference between the frequencies of natural oscillations predicted by MPCT and CT becomes less pronounced. The results suggest that higher modes exert a more substantial effect on material characteristics. Additionally, for a microplate with small thickness ($h=l_b$), the discrepancy between MPCT and CT

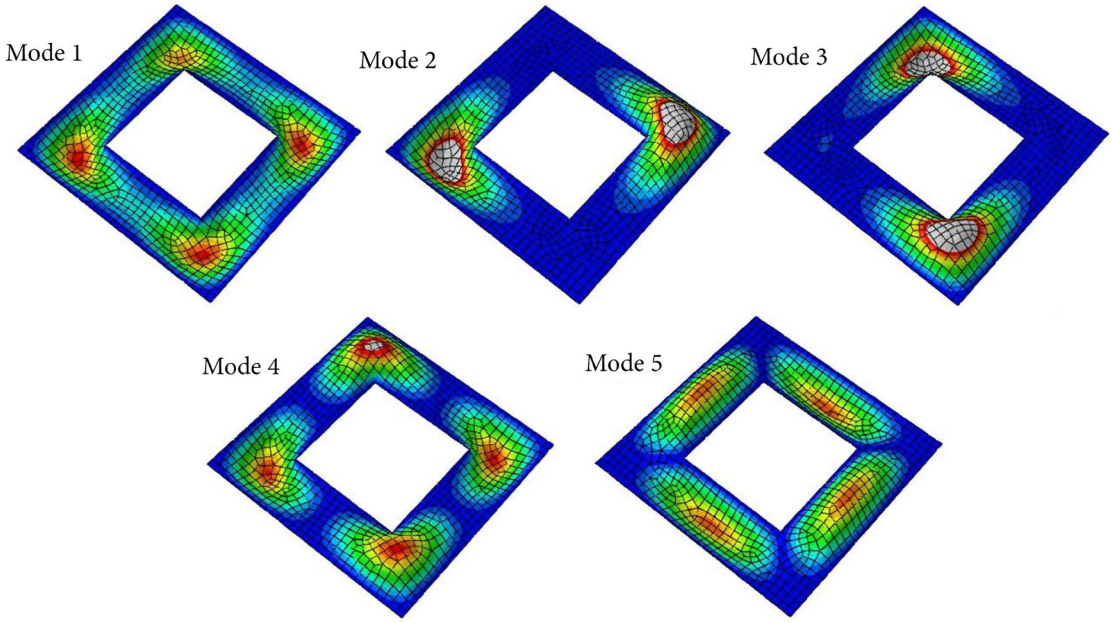

Figure12. Mode shapes of CC square microplate with a central hole.

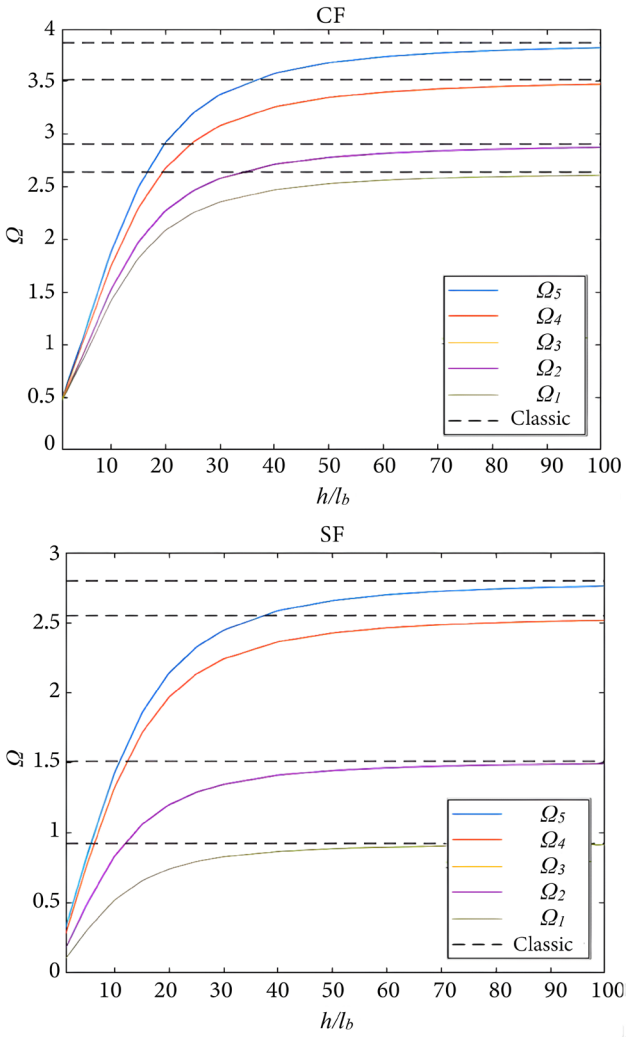

Figure 13. Non-dimensional natural frequencies of square microplate with a central hole discrepancy versus thickness-to-length scale ratio ($\frac{L}{h} = 10$).

frequencies is more prominent at higher modes than at lower modes.

Figures 14 and 15 depict the effect of boundary conditions and the side-to-thickness ratio ($\frac{L}{h}$) on the frequencies of natural oscillations for microplates with $\frac{h}{l_b} = 1$ and $\frac{h}{l_b} = 10$, respectively. These figures also include the corresponding classical frequencies. The frequencies of natural oscillations in various modes show an increase with higher $\frac{L}{h}$ ratios. The observed size effects on material characteristics are substantial, especially for large values of $\frac{L}{h}$, resulting in increased stiffness of the square micropolar plate.

6. Discussion and conclusion

Micro-Polar Continuum Theory (MPCT's) constitutive relations are first calculated using micropolar continuum mechanics to develop the element. The derived mass and stiffness matrices with micropolar effects for a non-classical quadrilateral plate were then obtained and directly implemented into MATLAB programming software. The proposed element applies to investigate three numerical examples under the different boundary conditions and geometries that correspond to the length-scale parameter. These examples demonstrate the advantages of the designed microplate. To explore the microplates' mechanical behavior, the influence of the length scale parameter is captured by the developed quadratic size-dependent plate element, which has three micro-rotational Degrees of Freedoms (DOFs) along with three traditional translational ones. It was concluded that when a microstructure's mesh is coarse, the adoption of higher-order plate theory tends to converge its frequencies more than once in earlier literature. Additionally, the non-

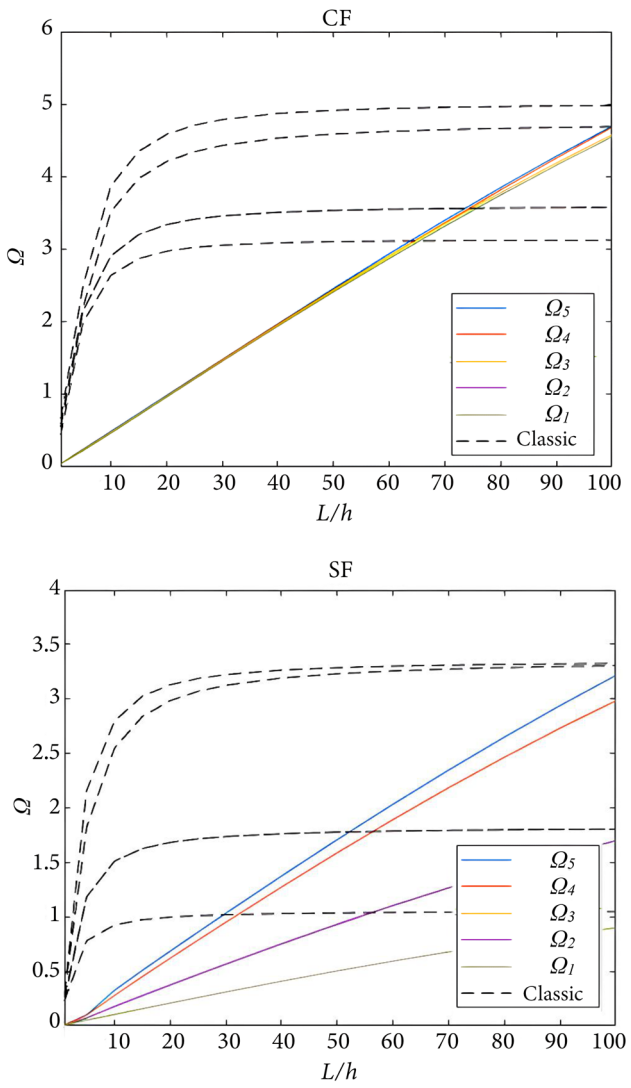

Figure 14. Non-dimensional natural frequencies of square microplate with a central hole discrepancy versus length-to-thick ness ratio ($\frac{h}{l_b} = 1$).

dimensional frequencies of natural oscillations of higher-order microplates demonstrated here closely match the analytical solutions, indicating that this model's geometry has a significant effect on the frequencies of natural oscillations of micropolar plates. When compared to other micropolar constants, the frequencies of the natural oscillations of microplates show that micro-inertia has a considerable effect. At small scales, the micropolar frequencies are also smaller than the classical ones. Furthermore, it appears that there is a noticeable change in the micropolar characteristics at higher modes since the discrepancy in frequencies between classical and micropolar plates increases with the mode number. However, it is shown that the results of the micropolar theory tend to resemble those of the classical theory at large values of h/l_b . In thick plates, unlike thin ones, the micropolar efficiency of the higher-order plate theory studied here can be concluded to diminish the difference between frequencies provided by the micropolar and the Classical Theories (CT) by increasing the

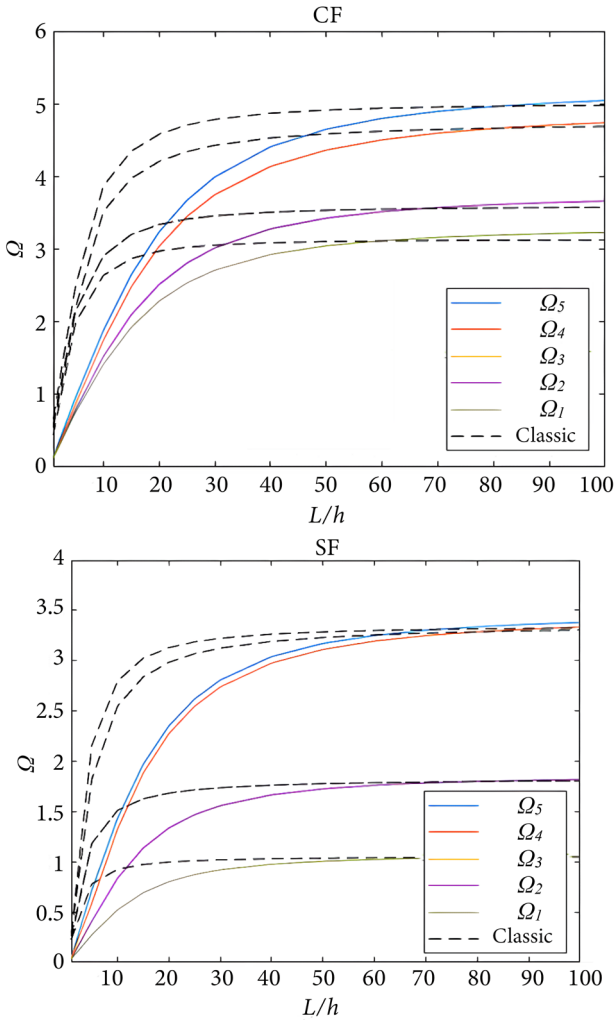

Figure 15. Non-dimensional natural frequencies of square microplate with a central hole discrepancy versus length-to-thickness ratio ($\frac{h}{l_b} = 10$).

side length-to-length scale ratio. The developed micropolar plate element has proven effective in capturing the mechanical behavior of microplates under various conditions. The study's insights into the influence of the length scale parameter, micro-inertia, and mode number on micropolar plate frequencies contribute to a better understanding of micropolar elasticity and its application in the analysis of microplates.

Nomenclature

$\tilde{\sigma}$	Classical stress tensor
$\tilde{\mu}$	Couple stress tensor
σ_{ij}	Components of the classical stress tensor
μ_{ij}	Components of the couple stress tensor
A_{ijkl} , $\overline{A}_{ijkl}$	Fourth-order tensors
I	Identity tensor
$\tilde{\varepsilon}$, $\tilde{\eta}$	Micro-strain tensors
γ	Micro-strain vector
γ_e	Micro-strain vector of the microplate element
$\hat{\varepsilon}$	Strain vector of a general microplate

$\tilde{e}$	Classical strain
ϕ	Micro-rotation vector
u	Displacement vector
λ , μ	Classical Lame coefficients
I_3	Three by three identity matrix
C	Elastic stiffness matrix
A , $\bar{A}$	Symmetric forms of the micropolar elastic stiffness matrices
K	Stiffness matrix
W	Strain energy of the microplate
W_e	Strain energy of the microplate element
δW	Variational form of the strain energy of the microplate
$\widehat{W}$	Strain energy density of the microplate
$\widehat{W}_e$	Strain energy density of the microplate element
T	Kinetic energy of the microplate
δT	Variational form of the Kinetic energy of the microplate
ρ	Mass density
f	Body force per unit mass
m	Body couple per unit mass
j	Micro-inertia per unit mass
l_b	Length scale parameter
l_t	Characteristic length (torsion)
L	Length of the microplate
h	Thickness of the microplate
ξ_1, ξ_2	Dimensionless coordinates in the plane of the plate
ξ_3	Dimensionless coordinate in the thickness direction
$u_{0_i}(\xi_1, \xi_2)$	Coordinates of the reference surface at the nodes
ω	Natural frequency
Ω	Dimensionless frequency of natural oscillation of the micropolar plate
E	Young modulus
G	Shear modulus
k_s	Shear correction factor
υ	Poisson's ratio
$\alpha, \beta, \gamma, \kappa$	Material constants of micropolar
$\in$	Permutation symbol
$\otimes$	Kronecker product symbol
H	Microbeam cross-section height
t	Time

Funding
This research did not receive any specific grant from funding agencies in the public, commercial, or not-for profit sectors.

Conflicts of interest
The authors declare no financial or personal conflicts of interest related to this work.

Authors contribution statement
All authors contributed to the reported work for conceptualization, methodology, validation, writing-review and editing, and supervision.

References
1. Hou, D., Wang, L., and Yan, J. "Vibration analysis of a cylindrical shell by using strain gradient theory via a moving Kriging interpolation-based meshfree method", *Thin-Walled Structures*, **184**, 110466 (2023). https://doi.org/10.1016/j.tws.2022.110466

2. Ahmad, F., Nazeer, M., Ali, W., et al. "Analytical study on couple stress fluid in an inclined channel", *Scientia Iranica*, **28**(4), pp. 2164-2175 (2021). https://doi.org/10.24200/sci.2021.55579.4291

3. Gholami, M. and Alizadeh, M. "A quasi-3D modified strain gradient formulation for static bending of functionally graded micro beams resting on Winkler-Pasternak elastic foundation", *Scientia Iranica*, **29**(1), pp. 26-40 (2022). https://doi.org/10.24200/sci.2021.55000.4019

4. Cosserat, E. and Cosserat, F. *Theorie des corps deformables*, Nature **81**(67) (1909). https://doi.org/10.1038/081067a0

5. Eringen, A.C. and Suhubi, E.S. "Nonlinear theory of simple microelastic solid, I and II", *International Journal of Engineering Science*, **2**(2), pp. 189-203 (1964). https://doi.org/10.1016/0020-7225(64)90004-7

6. Eringen, A.C., *Microcontinuum Field Theories: I. Foundations and Solids*, Springer Science and Business Media, New York (2012). https://doi.org/10.1007/978-1-4612-0555-5

7. Sargsyan, A.H. and Sargsyan, S.H. "Dynamic model of micropolar elastic thin plates with independent fields of displacements and rotations", *Journal of Sound and Vibration*, **333**, pp. 4354-4375 (2014). https://doi.org/10.1016/j.jsv.2014.04.048

8. Afsar Khan, A., Batool, R., and Kousar, N. "Examining the behavior of MHD micropolar fluid over curved stretching surface based on the modified Fourier law", *Scientia Iranica*, **28**(1), pp. 223-230 (2021). https://doi.org/10.24200/sci.2019.51472.2199

9. Nadeem, S., Amin, A., Abbas, N., et al. "Effects of heat and mass transfer on stagnation point flow of micropolar Maxwell fluid over Riga plate", *Scientia Iranica*, **28**(6), pp. 3753-3766 (2021). https://doi.org/10.24200/sci.2021.53858.3454

10. Eringen, A.C., *Theory of Micropolar Elasticity*, Liebowitz, Academic Press, New York, pp. 621-729 (1968). https://doi.org/10.1007/978-1-4612-0555-5_5

11. Daraei, B., Shojaee, S., and Hamzehei-Javaran, S. "Analysis of stationary and axially moving beams considering functionally graded material using micropolar theory and Carrera unified formulation", *Composite Structures*, **271**, 114054 (2021). https://doi.org/10.1016/j.compstruct.2021.114054

12. Aganovic´, I., Tambac˘a, J., and Tutek, Z. "Derivation and justification of the models of rods and plates from linearized three-dimensional micropolar elasticity", *Journal of Elasticity*, **84**(2), pp. 131-152 (2006). https://doi.org/10.1007/s10659-006-9060-6

13. Jeong, J. and Neff, P. "Existence, uniqueness and stability in linear Cosserat elasticity for weakest curvature conditions", *Mathematics and Mechanics of Solids*, **15**(1), pp. 78-95 (2008). https://doi.org/10.1177/1081286508093581

14. Bhattacharyya, A. and Mukhopadhyay, B. "Study of linear isotropic micro-polar plate in an asymptotic approach", *Computers and Mathematics with Applications*, **66**(6), pp. 1047-1057 (2013). https://doi.org/10.1016/j.camwa.2013.07.007

15. Altenbach, H. and Eremeyev, V.A. "Strain rate tensors and constitutive equations of inelastic micropolar materials", *International Journal of Plasticity*, **63**, pp. 3-17 (2014). https://doi.org/10.1016/j.ijplas.2014.05.009

16. Eremeyev, V.A. and Konopińska-Zmysłowska, V. "On dynamic extension of a local material symmetry group for micropolar media", *Symmetry*, **12**(10), 1632 (2020). https://doi.org/10.3390/sym12101632

17. Allman, D.J. "Evaluation of the constant strain triangular with drilling rotations", *International Journal for Numerical Methods in Engineering*, **26**, pp. 2645-2655 (1988). https://doi.org/10.1002/nme.1620261205

18. MacNeal, R.H. and Harder, R.L. "A refined four-noded membrane element with rotational degrees of freedom", *Computers and Structures*, **28**, pp. 75-84 (1988). https://doi.org/10.1016/0045-7949(88)90094-6

19. Hughes, T.J.R. and Brezzi, F. "On drilling degrees of freedom", *Computer Methods in Applied Mechanics and Engineering*, **72**, pp. 105-121 (1989). https://doi.org/10.1016/0045-7825(89)90124-2

20. Ibrahimbegovic, A., Taylor, R.L., and Wilson, E.L. "A robust quadrilateral membrane finite element with drilling degrees of freedom", *International Journal for Numerical Methods in Engineering*, **30**, pp. 445-457 (1990). https://doi.org/10.1002/nme.1620300305

21. Sangtarash, H., Arab, H.G., Sohrabi, M.R., et al. "A high-performance four-node flat shell element with drilling degrees of freedom", *Engineering with Computers*, **37**, pp. 2837-2852 (2021). https://doi.org/10.1007/s00366-020-00974-4

22. Altenbach, J., Altenbach, H., and Eremeyev, V.A. "On generalized Cosserat-type theories of plates and shells: A short review and bibliography", *Archive of Applied Mechanics*, **80**(1), pp. 73-92 (2010). https://doi.org/10.1007/s00419-009-0365-3

23. Yeh, J.T. and Chen, W.H. "Shell elements with drilling degree of freedoms based on micropolar elasticity theory", *International Journal for Numerical Methods in Engineering*, **36**, pp. 1145-1159 (1993). https://doi.org/10.1002/nme.1620360705

24. Huang, F.Y., Yan, B.H., Yan, J.L., et al. "Bending analysis of micropolar elastic beam using a 3-d finite element method", *International Journal of Engineering Science,* **38**, pp. 275-286 (2000). https://doi.org/10.1016/S0020-7225(99)00041-5

25. Ansari, R., Norouzzadeh, A., Shakouri, A.H., et al. "Finite element analysis of vibrating micro-beams and plates using three-dimensional micropolar element", *Thin-Walled Structures*, **124**. pp. 489-500 (2018). https://doi.org/10.1016/j.tws.2017.12.036

26. Kohansal-Vajargah, M. and Ansari, R. "Quadratic tetrahedral micropolar element for the vibration analysis of three-dimensional micro-structures", *Thin-Walled Structures*, **167**, 108152 (2021). https://doi.org/10.1016/j.tws.2021.108152

27. Kohansal Vajargah, M. and Ansari, R. "Vibration analysis of two-dimensional micromorphic structures using quadrilateral and triangular elements", *Engineering Computations*, **39**, pp. 1922-1946 (2022). https://doi.org/10.1108/EC-12-2020-0758

28. Natarajan, S., Ferreira, A., Bordas, S., et al. "Analysis of functionally graded material plates using triangular elements with cell-based smoothed discrete shear gap method", *Mathematical Problems in Engineering* (2014). https://doi.org/10.1155/2014/247932

29. Lakes, R. "Experimental microelasticity of two porous solids", *International Journal of Solids and Structures*, **22**, pp. 55-63 (1986). https://doi.org/10.1016/0020-7683(86)90103-4

30. Owen, D.R.J. and Hinton, E. *Finite Elements in Plasticity: Theory and Practice*, Pineridge Press, Swansea, U.K. (1980).

Biographies

Yazdan Alipour is a PhD student at Shahid Bahonar University of Kerman (SBUK), Kerman, Iran. He earned his MSc degree in Structural Engineering from Shahid Bahonar University, Iran in 2018 and his PhD degree in Structural Engineering from Shahid Bahonar University, Iran in 2024. He is interested in the computational micropolar continuum

theory and application to model and solve micro structural problems. In his doctoral thesis, main purpose was to develope numerical approaches for the analysis of dynamic problems based on the micropolar theory.

Saleh Hamzehei-Javaran has been an Associate Professor of Structural Engineering at Shahid Bahonar University of Kerman, Kerman, Iran since 2014 where he has been teaching theory of elasticity, theory of plates and shells, and continuum mechanics. He earned his BSc degree in Civil Engineering from Shahid Bahonar University, Iran in 2006, his MSc degree in Structural Engineering from Tarbiat Modares University, Iran in 2009, and his PhD degree in Structural Engineering from Tarbiat Modares University, Iran in 2013. He has published several papers in peer-reviewed national and international journals and conference articles. His research interests include boundary and finite element methods, computational mechanics, and wave propagation.

Saeed Shojaee has been a Professor of Structural Engineering at Shahid Bahonar University of Kerman, Kerman, Iran since 2008, where he has been teaching advanced engineering mathematics, nonlinear analysis, and control of structures. He earned his BSc degree in Civil Engineering from Shahid Bahonar University, Iran in 2001, his MSc degree in Structural Engineering from Iran University of Science and Technology, Iran in 2003, and his PhD degree in Structural Engineering from Iran University of Science and Technology, Iran in 2008. He has published numerous papers in peer-reviewed national and international journals and conference articles. His research interests include optimization techniques, finite and boundary element methods, and computational mechanics.